FARADAY

# Oxidative dehydrogenation of propane over rare-earth orthovanadates

**Chak-Tong Au[a]* and Wei-De Zhang[a,b]**
[a] *Department of Chemistry, Hong Kong Baptist University, Kowloon Tong, Hong Kong*
[b] *Department of Chemistry, Xiamen University, Xiamen 361005, P. R. China*

High-purity rare-earth orthovanadates ($R_EVO_4$), $PrVO_4$, $GdVO_4$, $DyVO_4$, $HoVO_4$, $ErVO_4$, $NdVO_4$, $TbVO_4$ and $LuVO_4$, have been prepared by the citrate method. XRD, FTIR, LRS, UV–VIS diffuse reflectance, TPR and EPR techniques have been employed to characterize them. The catalytic performances of $PrVO_4$, $ErVO_4$, $GdVO_4$, $DyVO_4$ and $NdVO_4$ in the oxidative dehydrogenation of propane can compete with that of $Mg_3V_2O_8$. The selectivity of propene over $TbVO_4$, $LuVO_4$ and $HoVO_4$ was relatively low. TPR results showed that the more easily the catalyst is reduced, the higher the propene selectivity. EPR and *in situ* Raman experiments confirmed the presence of low-valence vanadates at the catalyst surface in the reaction process. We observed that $^{18}O_2$-isotope exchange occurred over the catalysts *via* a double-step single exchange process and the activity of the catalysts increased with an increase of isotope exchange rate.



The utilization of relatively abundant and cheap alkanes in the chemical industry is always desirable. In the transformation of alkanes into valuable chemicals, selective oxidation is considered to be important.[1] VMgO was first reported to be active and selective in the oxidative dehydrogenation (OXD) of ethylbenzene.[2] Kung and co-workers discovered that the VMgO catalyst was also effective in the OXD of propane,[3–5] *n*-butane[3,6,7] and cyclohexane[8] and attributed the active phase to magnesium orthovanadate ($Mg_3V_2O_8$).[9] Three factors, *viz.* (i) the presence of tetrahedral $VO_4$, (ii) the absence of V=O double bonds and (iii) the difference in metallic vanadates, were pointed out to be responsible for the oxidative dehydrogenation properties of VMgO catalysts.[6,7,10] They also confirmed that due to the difference in alkane molecular structure and size, propane OXD to propene was active and selective on $Mg_3V_2O_8$ and α-$Mg_2V_2O_7$, whereas *n*-butane was only selective over $Mg_3V_2O_8$ but not over α-$Mg_2V_2O_7$.[9] In contrast to the suggestion of Kung and co-workers, Volta and co-workers and Guerrero-Ruiz *et al.* suggested that magnesium pyrovanadate (α-$Mg_2V_2O_7$) was the active and selective phase, whereas $Mg_3V_2O_8$ and $MgV_2O_6$ were phases responsible for total oxidation.[11,12] They compared the catalytic performances of pure α-$Mg_2V_2O_7$, $Mg_3V_2O_8$ and $MgV_2O_6$ in propane OXD with the reducibility and surface properties [characterized by XPS, EPR, electrical conductivity and nitrogen oxide (NO)–TPD] of the catalysts, and proposed that the presence of stable $V^{4+}$ ions and oxygen vacancies in α-$Mg_2V_2O_7$ are responsible for the high propene selectivity over α-$Mg_2V_2O_7$. In their opinion, the corner-sharing tetrahedral $VO_4$ structure in α-$Mg_2V_2O_7$ is more favourable for oxygen atom extraction than isolated tetrahedral $VO_4$ or octahedral $VO_6$ structures existing respectively in $Mg_3V_2O_8$ and $MgV_2O_6$. Such a difference in structure has been correlated to the catalytic performance of these three catalysts in oxidative dehydrogenation reactions.

Considering the chemical properties of rare-earth and alkaline-earth elements and with the aim to utilize rare-earth elements in the field of catalysis, we studied previously the pure phases of rare-earth orthovanadates $R_EVO_4$ ($R_E$ = Y, Ce, La, Nd, Sm, Eu) for the OXD of propane.[13] In this paper, we report further the preparation and characterization of other pure rare-earth orthovanadates $R_EVO_4$ ($R_E$ = Pr, Gd, Dy, Ho, Er, Nd, Tb, Lu) for the oxidative dehydrogenation of propane. Techniques such as BET surface-area measurements, XRD, IR, Raman, UV–VIS diffuse reflectance spectroscopy and EPR were employed to characterize the catalysts. Temperature programmed reduction (TPR), *in situ* Raman, NO–TPD and $^{18}O_2$-isotope exchange methods were used to probe the relationship between the catalytic activity and the nature of the catalysts.

## Experimental

### Catalyst preparation

$R_EVO_4$ ($R_E$ = Pr, Gd, Dy, Ho, Er, Nd, Tb, Lu) were prepared by the citrate method.[14] The starting materials were analytical grade $R_E(NO_3)_3 \cdot 5H_2O$ (Aldrich) and $NH_4VO_3$ (atomic ratio = 1 : 1). $R_E(NO_3)_3 \cdot 5H_2O$ and $NH_4VO_3$ (atomic ratio = 1 : 1) were first dissolved in deionized water and citric acid was then added in such a manner that the molar number of equivalent anions (three ions per molecule of citric acid) equalled that of the cations (total amount of $R_E^{3+}$ and $V^{5+}$). The resulting solution was heated on a steam-bath to obtain the solid which was heated at 400 °C for 24 h (to decompose the organic precursor) and then calcined at 550 °C for 6 h.

### Catalyst characterization

The structures of the prepared catalysts were confirmed by X-ray diffraction (XRD) using a Rigaku D/Max-RC instrument equipped with Cu-Kα radiation. The specific surface area of the catalysts was measured by the BET method of nitrogen adsorption at liquid-nitrogen temperature. FTIR spectra were recorded between 400 and 1200 $cm^{-1}$ with a Nicolet Magna-IR 550 spectrometer. Laser Raman spectroscopic (LRS) studies were performed on a Jobin Yvon U-1000 Raman spectrometer. UV–VIS diffuse reflectance spectra were recorded between 380 and 780 nm with a Shimadzu UV-2100 UV–VIS recording spectrophotometer. EPR was conducted on a Bruker 200D-SRC meter.

Temperature programmed reduction (TPR) was conducted by using 7% $H_2$–93% $N_2$ (v/v). The flow rate of the carrier gas was 20 ml $min^{-1}$ and a thermal conductivity detector was used. 40 mg of sample was used and the heating rate was 10 °C $min^{-1}$.

The NO–TPD and oxygen isotope exchange experiments were conducted in a flow system connected to a Hewlett Packard G1800A GCD mass quadrupole spectrometer. For the NO–TPD study, 200 mg of each sample was pretreated in a flow of pure He at 550 °C for 2 h and then cooled to 30 °C for NO adsorption. For the $^{18}O_2$-isotope exchange experiments, the sample was cooled to 200 °C and 10 μl $^{18}O_2$ (95–98%) was pulsed into the reactor. The procedures were

repeated at 300, 400, 500 and 600 °C. $^{16}O_2$, $^{16}O^{18}O$ and $^{18}O_2$ were monitored at the exit of the reactor to detect the oxygen exchange ability of each catalyst.

### Catalyst performance

Catalytic testing was conducted in a flow system. The sample (0.050 g) with particle size 35–75 mesh was placed in a fixed-bed (inner diameter 5 mm) quartz microreactor. Under standard conditions, the feed was composed of 10% $O_2$, 20% $C_3H_8$ and 70% He (v/v/v) and the total flow rate was 50 ml $min^{-1}$. An empty reactor showed no activity. All data were collected after 4 h of reaction.

The reaction products were analysed by on-line gas chromatography (Shimazu GC-8A equipped with C-R6A data processor) with helium as carrier gas. Two columns were used in parallel. A Porapak Q (60–80 mesh, Aldrich) column was used to separate the hydrocarbons and $CO_2$ while molecular sieves 5A were used to separate $O_2$ and CO. The column temperature was 100 °C. The conversion of propane was defined as (mole of propane consumed/mole of propane in feed) × 100% and the selectivity of product A was defined as (mole of product A/mole of propane consumed) × 100%/$R_C$ where $R_C$ is the ratio of the number of carbon atoms in propane to the number of carbon atoms in product A.

## Results and Discussion

### BET measurement

The specific surface areas of the prepared catalysts $R_EVO_4$ are listed in Table 1. The areas ranged from 12.2 to 44.8 $m^2$ $g^{-1}$. The catalysts can be divided into two groups. The surface areas of $ErVO_4$, $GdVO_4$ and $HoVO_4$ are higher (>32 $m^2$ $g^{-1}$) while that of the other five are lower (<22 $m^2$ $g^{-1}$). The difference in surface areas may affect the activity of the catalysts.

### X-Ray diffraction

Fig. 1 shows the XRD profiles of the $R_EVO_4$ catalysts. The results showed that high-purity tetragonal (zircon structure) $PrVO_4$, $GdVO_4$, $DyVO_4$, $HoVO_4$, $ErVO_4$, $NdVO_4$, $TbVO_4$ and $LuVO_4$ were obtained and no other phases were detected. The XRD spectra are in good agreement with the standard spectra of $PrVO_4$,[15] $GdVO_4$,[16] $DyVO_4$,[17] $HoVO_4$,[18] $ErVO_4$,[19] $NdVO_4$,[20] $TbVO_4$ [21] and $LuVO_4$.[22] The $d_{hkl}$ data of the prepared $R_EVO_4$ compared well with those of standards listed in the ASTM files (Table 2). The XRD line intensity of $TbVO_4$ is lower than those of the other catalysts, implying that crystallization of the compound was poor during preparation.

### FTIR study

Fig. 2 shows the FTIR spectra of the prepared $R_EVO_4$ samples. For all the $R_EVO_4$ studied, the strongest IR absorbance peak appears around 790–830 $cm^{-1}$. The strongest IR peaks for $GdVO_4$, $DyVO_4$ and $NdVO_4$ are close to each other (*ca.* 800 $cm^{-1}$). The most intense IR peak of $PrVO_4$ is at 797 $cm^{-1}$ while that of $LuVO_4$ is at 823 $cm^{-1}$. All the catalysts show two very weak peaks at 419 and *ca.* 450 $cm^{-1}$. The IR peaks and their assignments are given in Table 3. We noticed that there is a very weak peak at about 1020 $cm^{-1}$ in the IR spectra of $PrVO_4$, $DyVO_4$ and $NdVO_4$, which might be due to the presence of $V_2O_5$.[23]

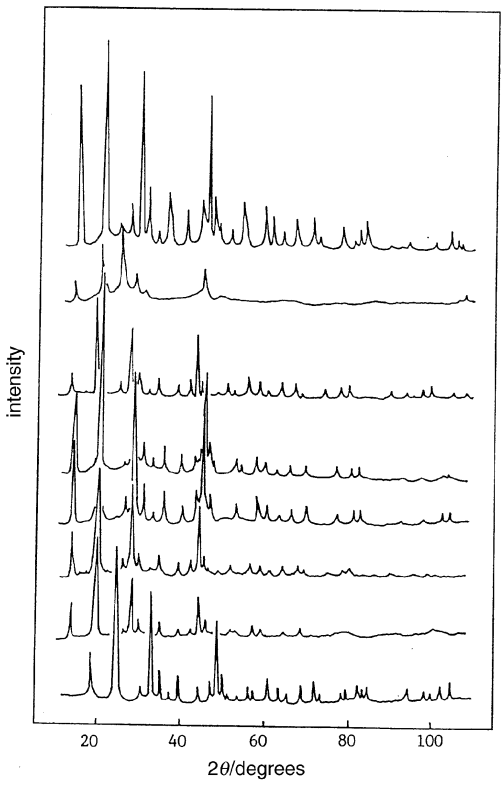


**Fig. 1** XRD profiles of $R_EVO_4$ (from bottom to top: $PrVO_4$, $GdVO_4$, $DyVO_4$, $HoVO_4$, $ErVO_4$, $NdVO_4$, $TbVO_4$ and $LuVO_4$)

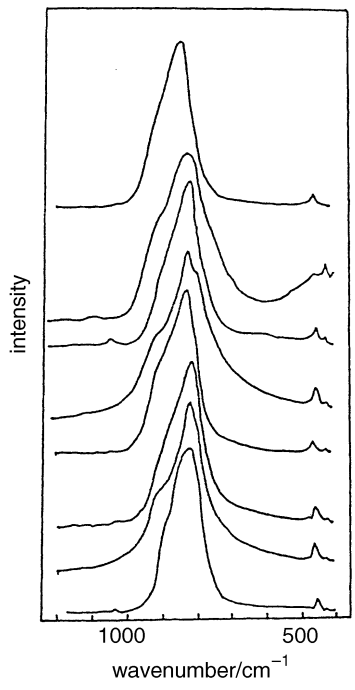


**Fig. 2** FTIR spectra of $R_EVO_4$ (from bottom to top: $PrVO_4$, $GdVO_4$, $DyVO_4$, $HoVO_4$, $ErVO_4$, $NdVO_4$, $TbVO_4$ and $LuVO_4$)

**Table 1** Specific surface areas of $R_EVO_4$

| catalyst | $PrVO_4$ | $GdVO_4$ | $DyVO_4$ | $HoVO_4$ | $ErVO_4$ | $NdVO_4$ | $TbVO_4$ | $LuVO_4$ |
|---|---|---|---|---|---|---|---|---|
| surface area/$m^2$ $g^{-1}$ | 13.8 | 43.1 | 14.6 | 32.8 | 44.8 | 12.2 | 18.7 | 21.8 |

**Table 2** $d_{hkl}$ Data from XRD of $R_EVO_4$ compared with the standards listed in ASTM files

| $PrVO_4$ | | $GdVO_4$ | | $DyVO_4$ | | $HoVO_4$ | | $ErVO_4$ | | $NdVO_4$ | | $TbVO_4$ | | $LuVO_4$ | | | | |
|---|---|---|---|---|---|---|---|---|---|---|---|---|---|---|---|---|---|---|
| *a* | *b* | *a* | *b* | *a* | *b* | *a* | *b* | *a* | *b* | *a* | *b* | *a* | *b* | *a* | *b* | *h* | *k* | *l* |
| 4.862(30) | 4.792(30) | 4.766(30) | 4.741(56) | 4.728(35) | 4.818(41) | 4.716(25) | 4.643(42) | 4.704(40) | 4.716(35) | 4.835(30) | 4.897(21) | 4.75(35) | 4.716(35) | 4.66(40) | 4.667(47) | 1 | 0 | 1 |
| 3.682(100) | 3.645(100) | 3.606(100) | 3.587(100) | 3.571(100) | 3.587(100) | 3.564(100) | 3.517(100) | 3.549(100) | 3.559(100) | 3.664(100) | 3.690(100) | 3.587(100) | 3.573(100) | 3.51(100) | 3.517(100) | 2 | 0 | 0 |
| 2.936(10) | 2.910(14) | 2.847(12) | 2.855(18) | 2.851(12) | 2.855(18) | 2.841(8) | 2.812(12) | 2.832(12) | 2.838(15) | 2.921(12) | 2.929(11) | 2.862(12) | 2.853(14) | 2.805(12) | 2.803(20) | 2 | 1 | 1 |
| 2.747(70) | 2.728(71) | 2.694(75) | 2.681(73) | 2.675(65) | 2.681(73) | 2.668(65) | 2.642(71) | 2.660(70) | 2.665(66) | 2.732(75) | 2.745(70) | 2.684(75) | 2.681(82) | 2.640(65) | 3.642(73) | 1 | 1 | 2 |
| 2.604(20) | 2.583(24) | 2.551(25) | 2.541(33) | 2.525(25) | 2.541(43) | 2.517(18) | 2.499(27) | 2.510(20) | 2.513(23) | 2.590(20) | 2.605(23) | 2.537(20) | 2.541(28) | 2.483(18) | 2.486(24) | 2 | 2 | 0 |
| 2.430(4) | 2.415(9) | 2.383(4) | 2.384(7) | 2.363(8) | 2.384(15) | 2.358(6) | 2.336(14) | 2.350(6) | 2.354(15) | 2.419(6) | 2.421(4) | 2.374(4) | | 2.330(4) | 2.331(8) | 2 | 0 | 2 |
| 2.295(16) | 2.280(19) | 2.248(12) | 2.236(14) | 2.227(12) | 2.236(14) | 2.221(16) | 2.205(23) | 2.213(18) | 2.215(21) | 2.284(16) | 2.296(16) | 2.238(18) | | 2.191(14) | 2.189(19) | 3 | 0 | 1 |
| 2.069(10) | 2.061(14) | 2.030(10) | 2.017(18) | 2.018(12) | 2.017(18) | 2.011(10) | 1.996(18) | 2.006(12) | 2.009(18) | 2.059(10) | 2.061(10) | 2.024(12) | | 1.992(10) | 1.992(15) | 1 | 0 | 3 |
| 1.947(10) | 1.940(17) | 1.908(12) | | 1.890(12) | | 1.884(10) | 1.872(20) | 1.878(12) | 1.879(17) | 1.938(12) | 1.944(15) | 1.899(12) | | 1.859(10) | 1.858(17) | 3 | 2 | 1 |
| 1.889(55) | 1.879(57) | 1.852(55) | 1.847(61) | 1.837(60) | 1.847(61) | 1.831(50) | 1.819(54) | 1.825(60) | 1.826(46) | 1.881(55) | 1.886(63) | 1.844(60) | 1.836(71) | 1.809(45) | 1.809(57) | 3 | 1 | 2 |
| 1.841(16) | 1.833(21) | 1.803(16) | | 1.786(14) | 1.796(16) | 1.781(16) | 1.767(23) | 1.775(18) | 1.776(22) | 1.832(16) | 1.836(18) | 1.794(16) | | 1.756(14) | 1.757(19) | 4 | 0 | 0 |
| 1.803(4) | 1.796(10) | 1.769(6) | 1.796(8) | 1.758(6) | | 1.751(4) | 1.735(10) | 1.746(4) | 1.751(14) | 1.795(6) | 1.796(5) | 1.763(6) | | 1.732(4) | 1.732(11) | 2 | 1 | 3 |
| 1.721(4) | 1.714(8) | 1.686(4) | | 1.671(6) | | 1.666(2) | | 1.660(4) | | 1.713(2) | 1.714(3) | 1.679(6) | | 1.643(4) | 1.643(9) | 4 | 1 | 1 |
| 1.647(12) | 1.641(16) | 1.613(12) | 1.609(14) | 1.597(14) | 1.609(18) | 1.593(10) | 1.581(15) | 1.587(12) | 1.589(17) | 1.639(14) | 1.641(14) | 1.606(12) | | 1.570(10) | 1.569(16) | 4 | 2 | 0 |
| 1.620(6) | 1.612(9) | | | | | 1.573(6) | 1.564(10) | | | 1.612(4) | 1.612(6) | 1.582(8) | | | | 3 | 0 | 3 |
| 1.617(6) | | 1.588(6) | | 1.579(6) | | | | | | | | | | | | | | |
| 1.529(12) | 1.524(19) | 1.499(16) | 1.496(21) | 1.486(12) | 1.496(16) | 1.481(14) | 1.472(17) | 1.568(6) | 1.568(14) | 1.609(6) | | | | 1.558(4) | 1.557(10) | 0 | 0 | 4 |
| 1.480(12) | 1.476(16) | 1.453(14) | 1.448(18) | 1.444(12) | 1.488(18) | 1.438(10) | 1.432(18) | 1.476(16) | 1.478(18) | 1.522(16) | 1.524(18) | 1.491(18) | | 1.462(12) | 1.462(16) | 3 | 3 | 2 |
| 1.435(6) | 1.432(10) | | | | | | | 1.434(14) | 1.436(17) | 1.473(14) | 1.476(13) | 1.447(14) | | 1.424(10) | 1.424(15) | 2 | 0 | 4 |
| | | | | | | | | | | | | 1.400(6) | | | | 5 | 0 | 1 |
| 1.373(10) | 1.368(15) | 1.348(10) | 1.340(17) | | | | | 1.330(12) | 1.330(16) | 1.367(12) | 1.369(14) | 1.342(12) | | 1.319(8) | 1.320(13) | 2 | 2 | 4 |

[a] ASTM files (ref. 15–22). [b] Present results.

**Table 3** Rare-earth orthovanadate FTIR peaks and their assigments[24]

| $PrVO_4$ | $GdVO_4$ | $DyVO_4$ | $HoVO_4$ | $ErVO_4$ | $NdVO_4$ | $TbVO_4$ | $LuVO_4$ | assignment |
|---|---|---|---|---|---|---|---|---|
| 419 vw | 419 vw | 419 vw | 419 w | | 419 vw | 419 vw | | |
| 446 w | 452 w | 447 w | 454 w | 453.5 w | 447 w | | 455 w | $\nu_S(VO_4)$ |
| 797 vs | 804 vs | 801 vs | 812 vs | 810 vs | 800 vs | 808 vs | 823 vs | $\nu_{AS}(VO_4)$ |
| | 901 (sh) | | 897 (sh) | 904 (sh) | | | 895 (sh) | $\delta_S(VO_4)$ |
| 1022 w | | 1018 vw | | | 1025 w | | | $\delta(V{=}O)$ |

## Raman study

The Raman spectra of the eight rare-earth orthovanadates are presented in Fig. 3 and the peaks are tabulated in Table 4. Compared with the other samples, the Raman peak of $TbVO_4$ is very weak. Similar to the Raman spectrum of $Mg_3V_2O_8$,[24] which has a very strong peak at 861 $cm^{-1}$, the spectra of $PrVO_4$, $GdVO_4$, $DyVO_4$, $HoVO_4$, $ErVO_4$, $NdVO_4$ and $LuVO_4$ also show a strong peak within the range 870–910 $cm^{-1}$. The spectrum of $TbVO_4$ only shows a weak peak at 888 $cm^{-1}$. $PrVO_4$ has another peak at 1000 $cm^{-1}$, while $HoVO_4$ and $NdVO_4$ have two peaks at around 706 and 1000 $cm^{-1}$, indicating that $V_2O_5$ was present as impurity.[23] Since the Raman cross-section of $V_2O_5$ is much larger than those of vanadates[24,25] and no $V_2O_5$ was detected in the XRD spectra, we believe that the amount of $V_2O_5$ impurity in the prepared $PrVO_4$, $DyVO_4$, $HoVO_4$ and $NdVO_4$ catalysts is extremely small.

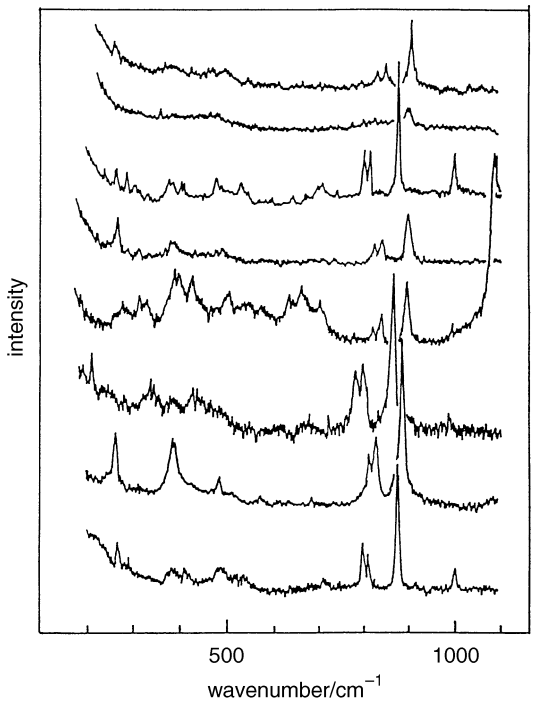


**Fig. 3** Raman spectra of $R_EVO_4$ (from bottom to top: $PrVO_4$, $GdVO_4$, $DyVO_4$, $HoVO_4$, $ErVO_4$, $NdVO_4$, $TbVO_4$ and $LuVO_4$)

## UV–VIS diffuse reflectance spectra

UV–VIS spectra of the $R_EVO_4$ samples have been recorded (Fig. 4). There are intense bands within the 550–800 nm range in the spectra of all the samples. Except for $GdVO_4$, $TbVO_4$ and $LuVO_4$, the spectra are split into two or three signals. $PrVO_4$ and $DyVO_4$ show a strong peak at 584 nm and a weak peak at 450 nm. $HoVO_4$ and $ErVO_4$ present a band at *ca.* 640 nm and three peaks at 513, 485 and 400 nm. $NdVO_4$ has a band at 731 nm and two peaks at 627 and 568 nm. The charge-transfer bands of vanadium (both $V^{5+}$ and $V^{4+}$) are reported to be in the range 300–500 nm,[26,27] while a typical d–d transition of $V^{4+}$ is in the range 700–800 nm. In our spectra, the bands within the 300–500 nm range are weak, while the bands within the 700–800 nm range are very strong. They may be attributed to $V^{4+}$ and rare-earth ions.

## Catalyst performance

The catalytic performances of the eight rare-earth vanadates in the oxidative dehydrogenation of propane were monitored. The major products were propene, CO and $CO_2$; no oxygenated product was observed. The carbon balance was found to be 97.5–101%. Table 5 shows the results of the catalytic OXD of propane at 500 °C. The results indicated that, except for $TbVO_4$ and $ErVO_4$, the $R_EVO_4$ catalysts were quite selective towards propene. The conversion of propane varied between 1.85 and 35.9%. The selectivity of propene ranged from 8.69 to 78.3%. $ErVO_4$ showed the highest propane conversion (35.9%), while $NdVO_4$ the lowest (1.85%). The $GdVO_4$ catalyst was both active and selective and the propene yield was high under the adopted testing condition. The $TbVO_4$ catalyst was the least selective of the eight catalysts. Since the conversion of propane over $TbVO_4$ was too low to be tested at a space velocity of 60 000 ml $h^{-1}$, a space velocity of 30 000 ml $h^{-1}$ was adopted. The propane conversion over $GdVO_4$, $HoVO_4$ and $ErVO_4$ was relatively higher than that over the other catalysts. This could be attributed to their high specific surface areas (Table 1). In order to present the catalytic behav-

**Table 4** Raman peaks of rare-earth orthovanadates

| $PrVO_4$ | $GdVO_4$ | $DyVO_4$ | $HoVO_4$ | $ErVO_4$ | $NdVO_4$ | $TbVO_4$ | $LuVO_4$ |
|---|---|---|---|---|---|---|---|
| | | | | | 148 s | | |
| 264 w | 264 m | | 284 vw | 264 m | | | |
| 288 vw | | | 318 vw | | | | |
| 378 vw | 392 m | | 392 w | 380 w | 386 w | | |
| 412 vw | | | 434 w | | 408 vw | | |
| 476 vw | 484 w | | 504 vw | | 476 vw | | |
| 528 vw | | | 640 vw | | 528 vw | | |
| | | | 664 vw | | | | |
| | | | 708 vw | | 706 w | | |
| 794 m | 812 m | 802 m | 822 w | 822 w | 798 m | | 832 w |
| 808 m | 830 m | 818 m | 842 m | 838 m | 812 m | | 850 m |
| 870 m | 888 s | 882 s | 898 s | 896 s | 874 s | 888 w | 904 s |
| 1000 w | | | 1000 w | | 1000 m | | |
| | | | 1096 vs | | | | |

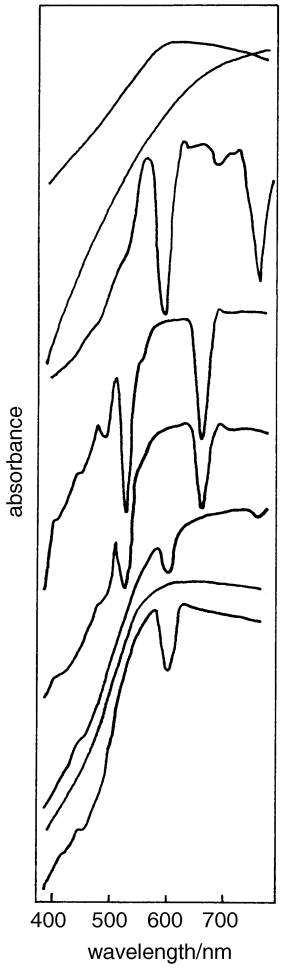


**Fig. 4** UV–VIS spectra of $R_EVO_4$ (from bottom to top: $PrVO_4$, $GdVO_4$, $DyVO_4$, $HoVO_4$, $ErVO_4$, $NdVO_4$, $TbVO_4$ and $LuVO_4$)

iour of the catalysts clearly, the selectivity as a function of conversion is plotted in Fig. 5. This shows that at similar propane conversion, the selectivities over the $PrVO_4$, $ErVO_4$, $GdVO_4$, $DyVO_4$ and $NdVO_4$ catalysts are similar, and are higher than that of $TbVO_4$, $LuVO_4$ and $HoVO_4$. The catalytic behaviour of the more active orthovanadates is comparable with that of $Mg_3V_2O_8$.[25]

### Temperature programmed reduction (TPR)

In order to examine the reducibility of the rare-earth orthovanadates, TPR experiments were conducted and the results are shown in Fig. 6. One can see that all the TPR profiles have a significant peak positioned within the range 680–760 °C and

**Table 5** Performance of rare-earth orthovanadates in propane OXD at 500 °C

| | | selectivity (%) | | | |
|---|---|---|---|---|---|
| catalyst | $C_3H_8$ conv. (%) | $C_3H_6$ | $CO_2$ | CO | $C_3H_6$ yield (%) |
| $PrVO_4$ | 2.17 | 78.3 | 7.70 | 14.0 | 1.70 |
| $GdVO_4$ | 7.28 | 61.5 | 16.0 | 22.5 | 4.48 |
| $DyVO_4$ | 4.35 | 67.5 | 16.3 | 16.2 | 2.94 |
| $HoVO_4$ | 12.4 | 45.0 | 19.5 | 35.5 | 5.58 |
| $ErVO_4$ | 35.9 | 22.4 | 22.6 | 55.0 | 8.04 |
| $NdVO_4$ | 1.85 | 76.9 | 9.79 | 13.3 | 1.42 |
| $TbVO_4$[a] | 9.31 | 8.69 | 60.0 | 31.3 | 0.08 |
| $LuVO_4$[b] | 6.62 | 53.5 | 17.6 | 28.8 | 3.54 |

Space velocity = 60 000 ml $g^{-1}$, except for [a] 12 000 ml $g^{-1}$ and [b] 30 000 ml $g^{-1}$.

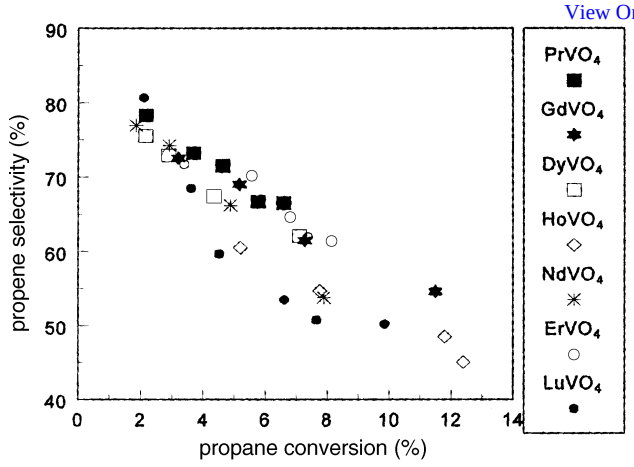


**Fig. 5** Relation of propene selectivity and the conversion of propane. Conditions: catalyst weight = 0.05 g, $T$ = 500 °C, $C_3H_8$ : $O_2$ : He = 20 : 10 : 70, total flow rate varied from 20 to 130 ml $min^{-1}$. The activity and selectivity of $TbVO_4$ were too low to be shown.

another small peak below 600 °C. We consider the peaks between 680 and 760 °C to be due to the reduction of $V^{5+}$ to $V^{3+}$. The peaks of lower intensity below 600 °C could be due to the reduction of surface species as XRD studies of the samples reduced up to 600 °C revealed no change in crystal structure. As confirmed by XRD, $R_EVO_4$ was reduced to $R_EVO_3$ after TPR treatment (Fig. 7 and Table 6). The XRD results also revealed that no apparent reduction of $R_E$ ions had occurred in the TPR process.

The different catalytic actions of the orthovanadates can be related to their redox properties. It has long been postulated that the catalytic activity and selectivity of an oxide in selective oxidation can be related to the reduction rate of the oxide. Over an oxide which is very difficult to reduce, the activity will be low; conversely for an oxide which is very easy to reduce, the activity is high but the selectivity low. An active and selective catalyst should have an intermediate ease of reduction.[28] Comparison of the propene selectivity over the catalysts (Fig. 5) with the temperature of the main TPR peaks (Fig. 6), leads to the observation of a correlation. The

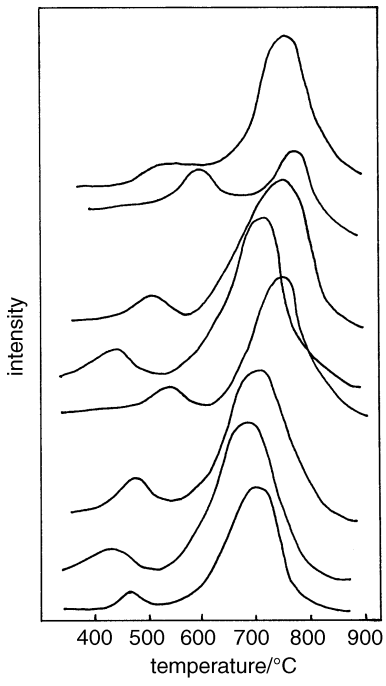


**Fig. 6** TPR profiles of $R_EVO_4$ (from bottom to top: $PrVO_4$, $GdVO_4$, $DyVO_4$, $HoVO_4$, $ErVO_4$, $NdVO_4$, $TbVO_4$ and $LuVO_4$)

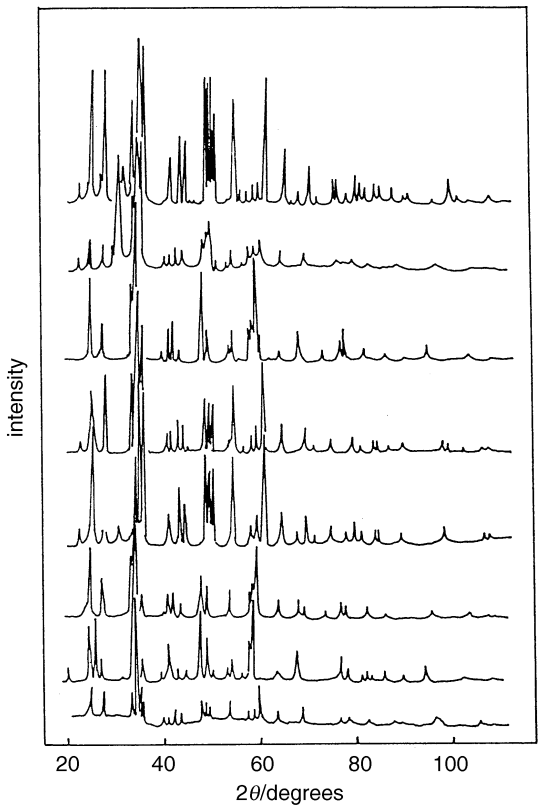


**Fig. 7** XRD profiles of $R_EVO_4$ after TPR (from bottom to top: $PrVO_4$, $GdVO_4$, $DyVO_4$, $HoVO_4$, $ErVO_4$, $NdVO_4$, $TbVO_4$ and $LuVO_4$), indicating $R_EVO_3$ formation

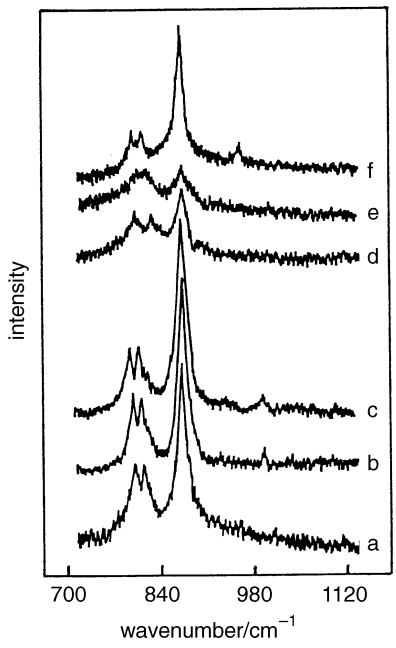


**Fig. 8** *In situ* Raman spectra of $DyVO_4$ treated at (a) 500 °C, $N_2$, (b) room temperature, $O_2$, (c) 200 °C, $10O_2$–$20C_3H_8$–$70N_2$, (d) 500 °C, $10O_2$–$20C_3H_8$–$70N_2$, 15 min, (e) 500 °C, $10O_2$–$20C_3H_8$–$70N_2$, 1 h and (f) 500 °C, $10O_2$–$70N_2$, 15 min



reduction peaks of $GdVO_4$, $ErVO_4$, $DyVO_4$, $PrVO_4$ and $NdVO_4$ occurred at lower temperature than those of $TbVO_4$, $LuVO_4$ and $HoVO_4$. The selectivity of propene over the former five catalysts was higher than that over the latter three, indicating that, in the present cases, the easier the reducibility of the orthovanadates, the higher the selectivity.

### *In situ* Raman study

*In situ* Raman experiments were performed to investigate changes in the catalysts after the oxidation reaction. Fig. 8 shows the Raman spectra of the $DyVO_4$ catalyst under different reaction conditions. The peak at about 875 $cm^{-1}$ is attributed to $VO_4$, while the peaks at 798 and 814 $cm^{-1}$ correspond to M–O–V.[24,29–31] The spectra do not noticeably change when the catalyst was treated up to 500 °C under an atmosphere of $N_2$ or $O_2$ (the peak at *ca.* 1000 $cm^{-1}$ is due to $V_2O_5$ impurity). Under the reactant mixture $10O_2$–$20C_3H_8$–$70N_2$ at 200 °C [Fig. 8(c)], the spectra did not change; however, after reaction at 500 °C for 15 min, the peaks at 798, 814 and 875 $cm^{-1}$ decreased in intensity. They were weakened further after 1 h reaction, indicating that the surface species had changed. The original spectrum could be restored by stopping the propane in the feed. The results clearly show that the vanadyl species on the catalyst surface had been reduced in the reaction process. We noticed that at the end of the reaction, the original colour of the catalysts changed from white or yellowish white (except for $NdVO_4$ which was greenish grey originally) to grey. This implies that the valence of V at the surface of the catalysts has changed from +5 to lower valence(s) (+4 or even +3). The XRD profiles of the catalysts after reaction nevertheless indicate that the rare-earth orthovanadates preserved their original structures. In other words, the bulk of the catalyst was stable during the reaction. The amount of low oxidation state vanadium was very small (not detectable by XRD). In the oxidation reaction, vanadium-based catalysts show $V^{5+}$–$V^{4+}$ and $V^{4+}$–$V^{3+}$ redox couples.[32] In the reaction of propane oxidative dehydrogenation over orthovanadates, we cannot confirm conclusively which couple is responsible for the dehydrogenation, but the low-valence V present at the surface of the catalysts seems to play an important role in the oxidative dehydrogenation process.

The Raman signal of $O_2^{2-}$ species is suggested to be within the range 730–950 $cm^{-1}$ while that of $O_2^-$ is at *ca.* 1164 $cm^{-1}$.[33,34] We could not identify signals due to $O_2^{2-}$ as there are vanadate peaks present within the 730–950 $cm^{-1}$ region. We did not observe any peak due to $O_2^-$ during the reaction.

### EPR and NO–TPD studies

Fig. 9 shows the EPR spectra of the $R_EVO_4$ catalysts and clearly reveals that the $V^{4+}$ ions were present in the catalysts. The $NdVO_4$, $HoVO_4$ and $TbVO_4$ samples show an intense signal with a $g$ value of about 1.98 which was assigned to $V^{4+}$ ions.[27] The $PrVO_4$, $DyVO_4$ and $ErVO_4$ samples show hyperfine structure due to $V^{4+}$ ($S = 1/2$; $I = 7/2$) in a distorted tetrahedral structure. The hyperfine structure is not particularly well resolved indicating that the $V^{4+}$ ions in the catalysts are not very far apart from each other. In other words, the concentration of $V^{4+}$ ions in the catalysts is not low. The $V^{4+}$ ions in the catalysts can be easily oxidized by $O_2$. Fig. 9(g) shows the EPR spectrum of $ErVO_4$ treated by $O_2$ at 550 °C for 10 min and then sealed in a glass tube. The spectrum shows that the EPR signal at $g = 1.98$ was greatly reduced.

The NO–TPD method can also be used to reveal the presence of $V^{4+}$ ions.[12] If there are $V^{4+}$ ions in the catalysts, chemically adsorbed NO can react with them at elevated temperatures. Two NO molecules react with a $V^{4+}$ ion to produce one molecule of $N_2O$. Since the desorption of $N_2O$ ($m/z = 44$) can be masked by $CO_2$, we first characterized the $CO_2$ desorption profile of the catalyst. Fig. 10(a) shows the $CO_2$ spectrum of the fresh $ErVO_4$ sample. There is a small shoulder at *ca.* 390 °C and the threshold for major $CO_2$ desorption is at 520 °C. Fig. 10(b) shows the NO–TPD of $ErVO_4$ pretreated by He at 550 °C for 2 h. The peak at *ca.* 440 °C corresponded to the release of $N_2O$ when NO reacts

**Table 6** $d_{hkl}$ Data of catalysts after TPR compared with the standards of $R_EVO_3$ listed in ASTM files

| $PrVO_3$ | | $GdVO_3$ | | $DyVO_3$ | | $HoVO_3$ | | $ErVO_3$ | | $NdVO_3$ | | $TbVO_3$ | | $LuVO_3$ | | | | |
|---|---|---|---|---|---|---|---|---|---|---|---|---|---|---|---|---|---|---|
| *a* | *b* | *a* | *b* | *a* | *b* | *a* | *b* | *a* | *b* | *a* | *b* | *a* | *b* | *a* | *b* | *h* | *k* | *l* |
| 3.89(16) | 3.864(19) | 3.86(16) | 3.897(21) | 3.84(16) | 3.860(24) | 3.83(14) | 3.815(23) | 2.82(20) | 3.831(16) | 3.9(20) | | 3.86(16) | 3.864(22) | 3.81(20) | 3.799(26) | 1 | 1 | 0 |
| | | 3.82(8) | | 3.80(12) | 3.820(13) | 3.78(8) | 3.767(15) | 3.78(14) | 3.783(11) | 3.87(15) | 3.880(24) | 3.81(12) | 3.799(14) | 3.77(16) | 3.756(19) | 0 | 0 | 2 |
| 3.48(6) | 3.457(9) | 3.45(18) | 3.490(9) | 3.43(14) | 3.450(15) | 3.42(20) | 3.411(24) | 3.41(20) | 3.424(20) | 3.481(10) | 3.477(12) | 3.447(20) | 3.437(23) | 3.398(20) | 3.386(25) | 1 | 1 | 1 |
| 2.765(25) | 2.759(17) | 2.802(20) | 2.835(16) | 2.796(16) | 2.786(22) | 2.795(20) | 2.795(18) | 2.79(18) | 2.795(20) | 2.787(30) | 2.786(21) | 2.802(20) | 2.803(23) | 2.784(16) | 2.778(15) | 0 | 2 | 0 |
| 2.749(100) | 2.742(100) | 2.717(100) | 2.745(100) | 2.702(100) | 2.278(100) | 2.696(100) | 2.688(100) | 2.688(100) | 2.696(100) | 2.746(100) | 2.745(100) | 2.712(100) | 2.712(100) | 2.678(100) | 2.673(100) | 1 | 1 | 2 |
| 2.736(30) | 2.733(25) | 2.672(25) | 2.682(7) | 2.648(25) | 2.666(24) | 2.636(35) | 2.620(38) | 2.628(40) | 2.635(31) | 2.725(45) | 2.726(37) | 2.664(25) | 2.665(43) | | | 2 | 0 | 0 |
| 2.606(5) | 2.607(9) | 2.630(12) | 2.641(7) | 2.625(18) | 2.620(10) | 2.623(1) | | | | 2.623(10) | 2.620(8) | 2.631(14) | 2.627(18) | 2.610(40) | 2.605(39) | 0 | 2 | 1 |
| 2.253(8) | 2.251(7) | 2.259(8) | 2.258(9) | 2.251(8) | 2.258(10) | 2.249(6) | 2.247(7) | 2.245(8) | 2.247(6) | 2.262(14) | 2.258(10) | 2.256(10) | 2.291(11) | 2.238(6) | 2.247(7) | 0 | 2 | 2 |
| 2.237(10) | 2.237(11) | 2.189(18) | 2.189(15) | 2.173(12) | 2.194(6) | 2.165(8) | 2.154(11) | 2.158(14) | 2.164(9) | 2.230(16) | 2.226(13) | 2.183(14) | 2.179(14) | 2.145(12) | 2.140(10) | 2 | 0 | 2 |
| 2.156(2) | | 2.127(10) | 2.129(6) | 2.115(10) | 2.125(6) | 2.110(10) | 2.102(9) | 2.105(10) | 2.111(8) | 2.152(6) | 2.149(5) | 2.122(10) | 2.121(11) | 2.095(12) | 2.092(9) | 1 | 1 | 3 |
| 1.945(14) | 1.938(18) | 1.934(25) | 1.947(22) | 1.924(25) | 1.938(22) | 1.919(18) | 1.913(16) | 1.912(20) | 1.916(18) | 1.948(30) | 1.947(23) | 1.931(22) | 1.928(20) | 1.902(18) | 1.901(13) | 2 | 2 | 0 |
| | | 1.910(18) | 1.898(15) | 1.899(16) | 1.902(13) | 1.894(16) | 1.886(13) | 1.890(14) | 1.890(13) | 1.935(18) | 1.936(13) | 1.905(16) | 1.901(29) | 1.883(16) | 1.879(12) | 0 | 0 | 4 |
| 1.891(5) | 1.905(11) | 1.884(14) | 1.890(15) | 1.877(16) | 1.883(14) | 1.874(12) | 1.868(9) | 1.870(12) | 1.872(9) | 1.893(12) | | 1.881(10) | 1.875(19) | 1.864(12) | 1.861(9) | 0 | 2 | 3 |
| 1.887(5) | 1.879(9) | 1.874(16) | 1.873(5) | 1.865(18) | 1.868(17) | 1.860(14) | 1.854(14) | 1.855(16) | 1.861(12) | 1.890(12) | 1.890(10) | 1.871(16) | 1.875(19) | 1.845(20) | 1.843(14) | 2 | 2 | 1 |
| 1.704(5) | 1.707(8) | 1.718(20) | 1.714(8) | 1.714(25) | 1.714(13) | 1.712(16) | 1.708(17) | 1.708(20) | 1.711(17) | 1.715(12) | 1.714(10) | 1.718(20) | 1.717(18) | 1.702(25) | 1.703(17) | 1 | 3 | 1 |
| 1.739(6) | | | | 1.597(8) | 1.581(8) | | | | | 1.741(4) | 1.732(6) | 1.722(3) | | 1.698(20) | 1.685(4) | 2 | 2 | 2 |
| 1.593(5) | | 1.601(8) | 1.599(11) | 1.571(14) | 1.572(20) | 1.595(6) | 1.591(5) | 1.591(6) | 1.594(5) | 1.601(12) | 1.599(8) | 1.601(6) | | 1.586(6) | 1.584(3) | 1 | 3 | 2 |
| 1.590(10) | 1.588(8) | 1.578(10) | 1.584(27) | | | 1.569(8) | 1.564(6) | 1.565(8) | 1.569(7) | 1.589(12) | 1.589(9) | 1.575(10) | 1.576(11) | 1.560(10) | 1.558(6) | 0 | 2 | 4 |
| 1.584(20) | 1.579(15) | 1.553(35) | 1.554(30) | | | 1.538(25) | 1.529(21) | 1.534(19) | 1.536(22) | 1.578(40) | 1.576(28) | 1.548(40) | 1.548(26) | 1.527(18) | 1.524(10) | 2 | 0 | 4 |
| 1.448(1) | | 1.450(10) | 1.454(6) | | | | | 1.439(10) | 1.442(8) | 1.454(6) | 1.454(4) | 1.448(10) | 1.448(13) | 1.432(12) | 1.434(8) | 1 | 3 | 3 |

[a] ASTM files (25-590, 25-205, 25-168, 25-295, 25-179, 25-547, 25-818, 25-468). [b] Present results.

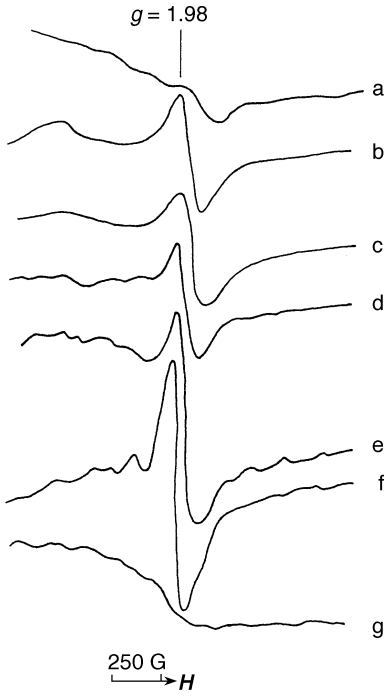


**Fig. 9** EPR spectra of (a) $TbVO_4$, (b) $NdVO_4$, (c) $HoVO_4$, (d) $PrVO_4$, (e) $DyVO_4$, (f) $ErVO_4$, and (g) $ErVO_4$ pretreated with $O_2$ at 550 °C

with $V^{4+}$. On the other hand, the NO–TPD of $ErVO_4$ pretreated by $O_2$ at 550 °C for 1 h has no peak in this range, indicating that the $V^{4+}$ ions have been oxidized by $O_2$ in the pretreatment process. This result is in good agreement with the EPR results.

### $^{18}O_2$-isotope exchange

$^{18}O_2$ has been employed to determine the degree of isotope exchange between gas-phase and lattice oxygen of the catalysts.[35] In our present study, the results obtained can be related solely to the exchange between gas-phase and lattice oxygen (so-called heterophase exchange), since blank experiments (without catalyst in the reactor) showed no occurrence of isotope exchange in the temperature range (200–600 °C) adopted in our investigation. In the experiments, catalysts were first pre-treated with pure He at 600 °C for 2 h before the admission of $^{18}O_2$. The observed isotope exchange must have occurred either *via* consecutive exchanges of gas-phase oxygen ($^{18}O_2$) with lattice oxygen ($^{16}O$) or through a single-step multiple exchange procedure.

Fig. 11 shows the result of $^{18}O_2$-isotope exchange over $GdVO_4$ and $ErVO_4$. It shows that the threshold temperature for the exchange of gaseous with lattice oxygen was about 420 °C. At any temperature above 420 °C, the amount of $^{16}O_2$ was much higher than that of $^{16}O^{18}O$, signifying that double exchange was dominant. The amount of $^{16}O_2$ increased linearly with increasing temperature while that of $^{16}O^{18}O$ was at a maximum at 500 °C and then decreased.

The double exchange of oxygen may be achieved by means of double-step single exchange:

$$^{18}O^{18}O(g) + |^{16}O| = {}^{18}O^{16}O + |^{18}O|$$

$$^{18}O^{16}O(g) + |^{16}O| = {}^{16}O^{16}O + |^{18}O|$$

or single-step double exchange:

$$^{18}O^{18}O(g) + 2|^{16}O| = {}^{16}O^{16}O + 2|^{18}O|$$

Here $|^{16}O|$ or $|^{18}O|$ represents lattice oxygen. It is considered that the $^{18}O_2$-isotope exchange is a result of thermo-equilibrium. We notice that the extent of double exchange is much larger than that of single exchange and the curve of single exchange exhibits a maximum at *ca.* 500 °C. The extent of double exchange reached approximately 100% at 600 °C. From these results, we deduce that double-step single exchange is the main process for $^{18}O_2$-isotope exchange over the catalysts.

Based on the EPR, NO–TPD, TPR, *in situ* Raman and

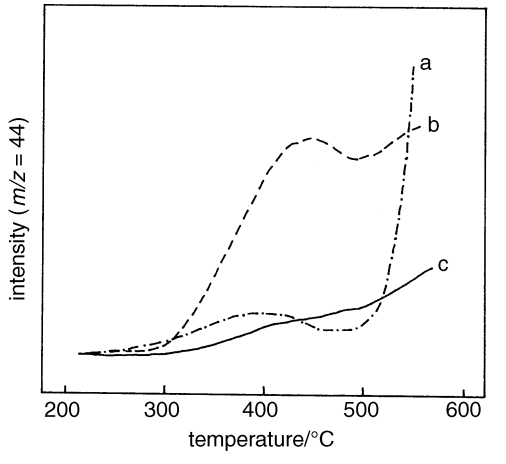


**Fig. 10** NO–TPD of $ErVO_4$: (a) $CO_2$ spectrum of a fresh sample, (b) $N_2O$ spectrum, sample pretreated with He at 550 °C for 2 h and (c) $N_2O$ spectrum, sample pretreated with $O_2$ at 550 °C for 1 h

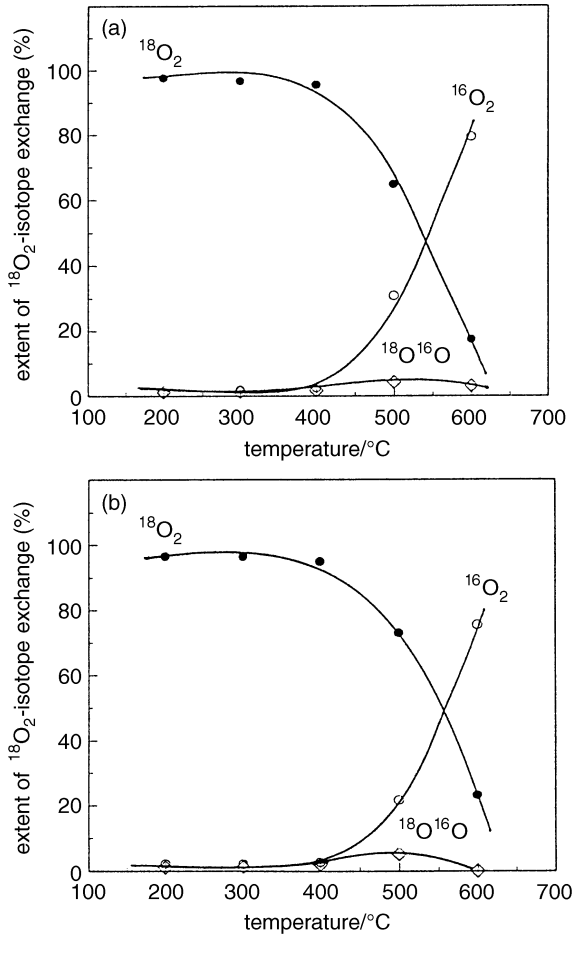


**Fig. 11** Result of $^{18}O_2$-isotope exchange over (a) $GdVO_4$ and (b) $ErVO_4$

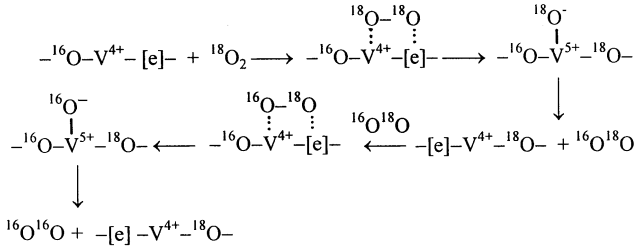

**Scheme 1**

catalytic performance results, we propose that there are oxygen vacancies and a very small amount of $V^{4+}$ in the catalysts. The $^{18}O_2$ molecule may react with the catalysts as shown in Scheme 1, where [e] represents an oxygen vacancy in the lattice of the catalysts. Since the amount of $|^{16}O|$ was much larger than that of $|^{18}O|$, the amount of single-exchange product $^{16}O^{18}O$ remained lower than that of double exchange. The single-exchange product increased initially due to the accumulation of exchanged $^{18}O$ in the lattice. However, upon an increase in the exchange rate with increasing temperature, there was a decline in single-exchange product above 520 °C.

From the analyses of the isotope exchange kinetics, one can reach the conclusion that the increase of the amount of $V^{4+}$ will result in the increase in $^{18}O_2$ exchange rate. We have reason to believe that the $^{18}O_2$-isotope exchange rate reflects the reaction activity: the oxidative dehydrogenation reaction was active at about 450 °C while the threshold temperature for $^{18}O_2$-isotope exchange was about 420 °C. At 500 °C, both the oxidative dehydrogenation of propane and isotope exchange processes became significant. Fig. 12 illustrates the relationship between the conversion of $^{18}O_2$ at 500 °C and the activity (conversion of propane at 500 °C) of the catalysts. It shows the trend that, the larger the extent of $^{18}O_2$ exchange, the higher the catalytic activity. It is reasonable to suggest that the $V^{4+}$ ions are involved in the activation of $O_2$, resulting in the generation of active oxygen species such as $O^-$ and adsorbed dioxygen. These surface oxygen species promote the oxidative dehydrogenation of propane.

## Conclusion

The results of XRD, LRS and IR investigations show that pure rare-earth metal orthovanadates can be prepared conveniently by the citrate method. No impurity was detected by XRD in all of the eight prepared catalysts; the more sensitive IR and Raman techniques, however, showed that there was a small amount of $V_2O_5$ impurity in the $PrVO_4$, $DyVO_4$, $HoVO_4$ and $NdVO_4$ catalysts. The prepared $R_EVO_4$ catalysts were active and selective in the oxidative dehydrogenation of propane. The catalytic performances of $PrVO_4$, $ErVO_4$, $GdVO_4$, $DyVO_4$ and $NdVO_4$ in the oxidative dehydrogenation of propane are similar to that of $Mg_3V_2O_8$. The catalytic performance of the rare-earth orthovanadates can be related to the redox properties as well as to the surface properties of the catalysts. EPR, NO–TPD, *in situ* Raman and $^{18}O_2$-isotope exchange results strongly indicate that the low-valence vanadates present were playing an important role in the dehydrogenation process.

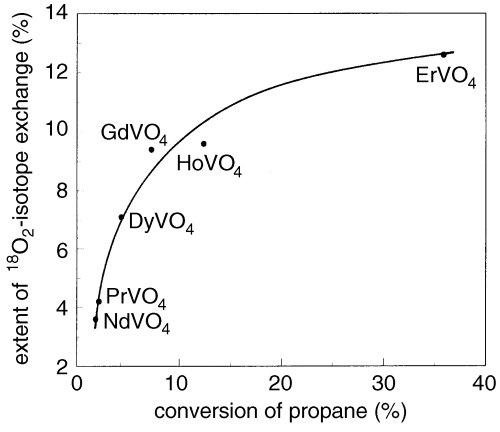


**Fig. 12** The relationship between the extent of $^{18}O_2$-isotope exchange and the conversion of propane at 500 °C over $R_EVO_4$ catalysts

The authors gratefully acknowledge the support of this work by the Hong Kong Research Grants Council, UGC (HKBC 102/93E) and the State Key Laboratory for Physical Chemistry of Solid Surface in Xiamen University, P. R. China, for the facilitation of the LRS, UV–VIS spectra and EPR measurements.

## References

1 A. T. Bell, M. Boudart and B. D. Ensley, *Catalysis Looks to the Future*, National Academy Press, Washington, DC, 1992, p. 21.
2 J. Hanuza, B. Jezowska-Trzeblatowska and W. Oganowski, *J. Mol. Catal.*, 1985, **29**, 109.
3 H. H. Kung and M. A. Chaar, *US Pat.*, 4,722,319, 1988.
4 M. A. Chaar, D. Patel and H. H. Kung, *J. Catal.*, 1988, **109**, 463.
5 K. T. Nguyen and H. H. Kung, *J. Catal.*, 1990, **122**, 415.
6 M. A. Chaar, D. Patel, M. C. Kung and H. H. Kung, *J. Catal.*, 1987, **105**, 483.
7 D. Patel, P. J. Andersen and H. H. Kung, *J. Catal.*, 1990, **125**, 132.
8 M. C. Kung and H. H. Kung, *J. Catal.*, 1991, **128**, 287.
9 P. M. Michalakos, M. C. Kung, I. Jakan and H. H. Kung, *J. Catal.*, 1993, **140**, 226.
10 O. S. Owen, M. C. Kung and H. H. Kung, *Catal. Lett.*, 1992, **12**, 45.
11 D. S. H. Sam, V. Soenen and J. C. Volta, *J. Catal.*, 1990, **123**, 417.
12 A. Guerrero-Ruiz, I. Rodriguez-Ramos and J. L. G. Fierro, *Stud. Surf. Sci. Catal.*, 1992, **72**, 203.
13 C. T. Au, W. D. Zhang and H. L. Wan, *Catal. Lett.*, 1996, **37**, 241.
14 P. Courty, H. Ajot, C. Marcilly and B. Delmon, *Powder Technol.*, 1973, **7**, 21.
15 *Natl. Bur. Stand. US Monogr.*, 1967, **25**, 25 40, ASTM file No. 17-879.
16 *Natl. Bur. Stand. US Monogr.*, 1967, **25**, 5 30, ASTM file No. 17-260.
17 *Natl. Bur. Stand. US Monogr.*, 1966, **25**, 25 15, ASTM file No. 16-870.
18 *Natl. Bur. Stand. US Monogr.*, 1966, **25**, 4 18, ASTM file No. 15-764.
19 *Natl. Bur. Stand. US Monogr.*, 1967, **25**, 25 29, ASTM file No. 17-199.
20 *Natl. Bur. Stand. US Monogr.*, 1966, **25**, 30, ASTM file No. 15-769.
21 *Natl. Bur. Stand. Rep.*, 1965, July, 8944, ASTM file No. 17-340.
22 *Natl. Bur. Stand. US Monogr.*, 1966, **25**, 25 37, ASTM file No. 17-880.
23 C. Cristiani, P. Forzatti and G. Busca, *J. Catal.*, 1989, **116**, 586.
24 X. Gao, P. Ruiz, X. Guo and B. Delmon, *Catal. Lett.*, 1994, **23**, 321.
25 X. Gao, P. Ruiz, Q. Xin, X. Guo and B. Delmon, *J. Catal.*, 1994, **148**, 56.
26 E. Bordes and P. Courtine, *J. Catal.*, 1979, **57**, 236.
27 G. Martini, F. Trifiro and A. Vaccarl, *J. Phys. Chem.*, 1982, **86**, 1573.
28 V. D. Sokolovskii, *Catal. Rev. Sci., Eng.*, 1990, **32**, 1.
29 P. M. Michalakos, K. Birkeland and H. H. Kung, *J. Catal.*, 1996, **158**, 349.
30 P. J. Andersen and H. H. Kung, *J. Phys. Chem.*, 1992, **96**, 3114.
31 G. T. Went, S. T. Oyama and A. T. Bell, *J. Phys. Chem.*, 1990, **94**, 4240.

32 G. Busca, F. Cavani, G. Centi and F. Trifiro, *J. Catal.*, 1986, **99**, 400.
33 H. H. Eysel and S. Thym. *Anorg. Allg. Chem.*, 1975, **411**, 97.
34 M. Bosch and W. Kanzig, *Helv. Phys. Acta*, 1975, **48**, 743.
35 Y-F. Chang, G. A. Somorjai and H. Heinemann, *J. Catal.*, 1993, **142**, 697.

*Paper* 6/07565G; *Received* 6*th November*, 1996